




Electronic Bands and Dielectric Functions of $\text{In}_{0.5}\text{Tl}_{0.5}\text{I}$ Solid State Solution with Structural Defects

B. ANDRIYEVSKY ^{1,8} A.I. KASHUBA,^{2,3} I.M. KUNYO,³
K. DORYWALSKI,⁴ I.V. SEMKIV,⁵ I.V. KARPA,³ V.B. STAKHURA,²
L. ANDRIYEVSKA,⁶ J. PIEKARSKI,⁶ and M. PIASECKI⁷

1.—Faculty of Electronics and Computer Sciences, Koszalin University of Technology, Śniadeckich str. 2, 75-453 Koszalin, Poland. 2.—Faculty of Physics, Ivan Franko National University of Lviv, Cyryl and Metody str. 8a, Lviv 79005, Ukraine. 3.—Faculty of Electronics and Computer Technologies, Ivan Franko National University of Lviv, Tarnavsky str. 107, Lviv 79005, Ukraine. 4.—Faculty of Technology and Education, Koszalin University of Technology, Śniadeckich str. 2, 75-453 Koszalin, Poland. 5.—Faculty of Physics, Lviv Polytechnic National University, S. Bandera str. 12, Lviv 79013, Ukraine. 6.—Faculty of Civil Engineering, Environmental and Geodetic Sciences, Koszalin University of Technology, Śniadeckich str. 2, 75-453 Koszalin, Poland. 7.—Institute of Physics, Jan Długosz University Czestochowa, Armii Krajowej str. 13/15, Czestochowa, Poland. 8.—e-mail: bohdan.andriyevskyy@tu.koszalin.pl

We investigate an influence of the crystal structure imperfections on the electronic properties and dielectric functions of the $\text{In}_{0.5}\text{Tl}_{0.5}\text{I}$ semiconductor in the frame of the density functional theory calculations. The tensor of electron effective mass m_{ij}^* for the InI , $\text{In}_{0.5}\text{Tl}_{0.5}\text{I}$ and TlI crystals has been calculated for the valence and conduction bands at different K -points of the Brillouin zone. The dielectric functions $\epsilon(h\nu)$ of the imperfect crystals based on $\text{In}_{0.5}\text{Tl}_{0.5}\text{I}$ solid state solution with iodine vacancy and a thallium interstitial atom were calculated taking into consideration the inter-band and intra-band electron transitions. The studies of the imperfect crystals reveal increased low-frequency and stationary electron conductivity with anisotropy resulted from the anisotropy of the electron effective mass tensor. Our findings explain the origin of crucial changes in the band structure by formation of the donor half-occupied levels close to the unoccupied conduction bands due to the crystal structure defects, i.e., iodine vacancy or a thallium interstitial atom. It has been shown that in the case of real crystals, in particular metal-halides, the proper consideration of defects in quantum-chemical calculations results in a better matching with experimental data and, opposite to the perfect structure calculations, gives opportunities to explain the observed phenomena.

Key words: Semiconductors, band structure, effective mass, dielectric function, electron conductivity

INTRODUCTION

The searching for the new functional materials with tunable physical properties is of key interest for current micro and optoelectronics. Over the past few decades the attention of scientists is being

focused on those new materials that offer possibilities to tune their physical properties in a controllable way. This can be achieved in many ways by modifications of initial materials to meet the desirable properties suitable for potential applications.

One of these novel modifications is the insertion of the modified bow-tie particles consisting of a pair of opposing metallic truncated triangles, embedded in a dielectric environment, with a rectangular dielectric hole engraved on the metallic structure. The

modified bow-tie nanoparticles method may be used in biomedical applications.¹

Another possible modification of materials is their doping by certain chemical elements to achieve the corresponding refractive index close to zero in the infrared or visible spectral ranges. Such near-zero refractive index materials may be used for the purpose of light beam handling in the optoelectronic devices.² The main physical consequences of such method of the materials properties modification may be better understood and properly modelled by using the density functional theory (DFT) based theoretical studies of the structural, energetic and electronic properties of these modified materials. The results of the present study for the titled crystals fall into this category.

Another approach to control and manipulate the materials properties for different electromagnetic sensors is the use of the meta-surfaces, which represent the artificial low-dimensional materials with the spatial periodicity much smaller than the operative wavelength. This method is sufficiently universal and was applied to develop devices for advanced sensing and medical diagnostic applications showing improved performance in terms of sensitivity and selectivity.³

In the last decade, many studies have been devoted to the graphene applications in the optoelectronic devices. It has been shown that one can have the graphene platform for infrared meta-materials and transformation optical devices. Variation of the applied electric field allows for tuning the graphene conductivity in the terahertz and infrared frequency ranges, that permits to realize numerous photonic functions and meta-material concepts on such basis.⁴

The known phenomenon to control and change the parameters of the electromagnetic waves in materials is the surface plasmon resonance (SPR). SPR is the resonant oscillation of conduction electrons at the interface between negative and positive electric permittivity materials (metal and insulator) stimulated by incident light. Distribution of the optical waves along such interface may be studied theoretically using the Green function approach, that permits to obtain necessary parameters for the realization of different functional devices.⁵

One of the popular and effective methods to tune the electronic and optical properties of a material is a gradual substitution of one of the crystal's components by another chemical element from the same or similar group of the periodic system. Such a procedure introduces internal stress into the crystal (mostly caused by the mismatch of ionic radii of the chemical elements involved) and leads to the formation of the solid state solutions (SSS).^{6,7} So far, we have successfully tuned the properties of several crystals by changing chemical composition and utilizing structure-properties relations for such modified compounds, using both experimental methods and computer simulations.^{8–10}

It is well known that during crystal growth processes all kinds of defects always appear: twinings, interstitials, vacancies or atomic positions exchange.¹¹ The structural defects substantially affect the electronic structure of a material, they change the optical properties, transport phenomena and finally influence its structural stability. In many cases, the controlled level of certain defects may enhance the desired properties of materials such as non-linear optical, thermoelectric, etc. Existence of widely available DFT-based computational methods made easier theoretical studies of the defect-containing materials. However, quite often, significant differences between the experimental and calculated data can be encountered. This situation is not only because of the limitations of the applied theoretical models or computational techniques (e.g., the well-known underestimation of the band gap obtained with using the DFT) but because of not taking into account defects existing in real crystals. In the present study, the influence of crystal structure deviations of the ternary crystals $\text{In}_x\text{Tl}_{1-x}\text{I}$ and its solid solutions from the perfect one on the corresponding electronic properties was computationally investigated by using the DFT approach. Comparison of the computational results obtained in the present investigation with our previous experimental and theoretical studies of the same materials confirms the effectiveness of the structure defects models adopted. The method proposed in this work can be extended to modeling and prediction of the properties of new crystalline materials or to verify validity of the calculations made with the assumption of a perfect structure and corresponding experimental data.

Thallium, embedded in a stable crystal matrix, having saturated bonds, is not as dangerous as a free atom or ion, while the chemical compounds that contain it possess extremely interesting optical properties^{8,9} and are excellent thermoelectric materials.¹² Among the mixed semiconductors of the $\text{A}^{\text{III}}\text{B}^{\text{VII}}$ group, the three-component crystals $\text{In}_x\text{Tl}_{1-x}\text{I}$, representing a continuous series of SSS, may be promising for applications in optoelectronics in spite of already known investigations of these SSS many years ago.^{13–15} Their band gap E_g varies within the 2.01–2.84 eV range.^{13–16} The crystals possess a layered structure. However, in contrast to typical layered crystals of the $\text{A}^{\text{II}}\text{B}^{\text{VII}}$ and $\text{A}^{\text{III}}\text{B}^{\text{VI}}$ (CdI_2 , HgI_2 , GaSe , InSe) groups,^{17,18} in which the van der Waals interlayer gaps are formed mainly by the corresponding anions, in $\text{In}_x\text{Tl}_{1-x}\text{I}$ SSS, this weakest chemical bonding is probably created by indium and thallium cations and iodine anions. Investigations of the $\text{In}_x\text{Tl}_{1-x}\text{I}$ crystals are of interest because such samples combine properties of both InI and TlI . The application prospect of these compounds is associated with their use as materials in the ionizing radiation detectors and optical modulators of CO_2 laser.¹⁹

The crystal structure of TII was firstly investigated at ambient temperature²⁰: number of formula units per unit cell $Z = 4$, orthorhombic space group No. 63 *Cmcm*, lattice constants (all in Å) $a = 4.57$, $b = 12.92$, $c = 5.24$. In turn, the crystal structure of InI has been determined as follows^{21,22}: InI, structure type TII, $Z = 4$, orthorhombic space group No. 63 (*Cmcm*), $a = 4.763$, $b = 12.781$, $c = 4.909$. The space group of symmetry for InI crystal is the same as for TII one.

Thallium iodide crystallizes in a rhombic structure at the temperatures up to 178°C, but at higher temperatures, it transforms into the CsCl structure of the cubic symmetry.²³ In halides of indium, no phase transitions occur except in InCl. The crystals InI and TII cleave perpendicularly to the crystallographic b -axis.^{13–18} Smooth controlled changes of the energy band gap E_g , mechanical and photovoltaic characteristics and spectral range of the recombination radiation may be realized in them. Results of investigation of the band structure and photoconductivity with change of the indium versus thallium content of the crystals $\text{In}_x\text{Tl}_{1-x}\text{I}$ are presented in the recent study.¹⁶

So far, studies of the phonon spectra, mechanical and optical characteristics are known for $\text{In}_x\text{Tl}_{1-x}\text{I}$ SSS.^{24–27} In Ref. ²⁴ a possibility of forming the InI structure as a matrix for the TII quantum dots inclusion is discussed. The reduction of the crystal unit cell dimensions b and c , and the unit cell volume V and the increase of dimension a together with the increase of content index x are the main features indicating the continuous structure changes of $\text{In}_x\text{Tl}_{1-x}\text{I}$ ¹⁶ (in the previous Refs. ^{13–18} and ^{22–27} the convention $a \approx c < b$ for the unit cell dimension was adopted).

The optical anisotropy, which is expected due to the layered structure, and the continuous structure transformations mentioned above make $\text{In}_x\text{Tl}_{1-x}\text{I}$ SSS a perspective for the nonlinear optics and electrical engineering applications. For this purpose, the details of the phenomena associated with such applications of $\text{In}_x\text{Tl}_{1-x}\text{I}$ SSS should be studied. In particular, it was found¹⁶ that the photoconductivity spectra in the ac layer of $\text{In}_x\text{Tl}_{1-x}\text{I}$ SSS correspond to the n - and p -types carriers. It was also suggested that the appearance of the n -type conductivity, occurred primarily in the a -crystallographic direction of $\text{In}_x\text{Tl}_{1-x}\text{I}$, is caused by the anionic vacancy or cationic interstitials. If an alternation of the conductive and insulating sub-layers along the b unit cell dimension of the crystal is possible, one can assume that $\text{In}_x\text{Tl}_{1-x}\text{I}$ SSS may be used as a material for the low-dimensional capacitors. From this point of view, one of the main goals of this work is to study the origin of electric conductivity and the quasi-metallization of $\text{In}_x\text{Tl}_{1-x}\text{I}$ SSS.

If the suggested anionic vacancies or cationic interstitials in $\text{In}_x\text{Tl}_{1-x}\text{I}$ SSS lead to the quasi-metallization, this should be revealed in the band

structure and dielectric function of the material. The present study is based on the first principles calculations in the framework of the DFT of the band structure and dielectric functions of the nominally pure crystal $\text{In}_{0.5}\text{Tl}_{0.5}\text{I}$ and on the changes of these characteristics caused by the anionic vacancies and cationic interstitials in the compound.

METHODS OF CALCULATIONS

Different theoretical methods may be applied to study the propagation of electromagnetic waves in dielectric materials: the effective medium theory,²⁸ the multi-layer approach,²⁹ and the multi-resonances based on the modified metallic nanoparticles.³⁰ These methods, however, are related to the studies mainly of the relatively large inhomogeneities in dielectric materials. In the present study, the properties of the titled crystals, derived from the corresponding interatomic bonding, were calculated in the framework of the DFT.³¹

Calculations of band structure and related properties of the materials were carried out using the academic CASTEP code.³² The calculations were performed within the generalized gradient approximation (GGA) with the Perdew–Burke–Ernzerhof (PBESOL) exchange-and-correlation functional.³³ The interaction of electrons with atomic cores was described with the norm-conserving pseudopotentials supplied with the academic CASTEP.³² It is well known that in most cases this method causes a lowering of the band gap value E_g , which may be corrected by using the “scissors” operator or by taking into account the strong correlation of d -electrons, if the later ones participate in large amount in the forming of the band gap E_g .

The electronic wave functions are expanded in a plane wave basis set with the energy cut-off of 650 eV. The atomic levels $4d^{10}5s^25p^1$ for indium, $5d^{10}6s^26p^1$ for thallium and $5s^25p^5$ for iodine atoms are treated as valence electron states. For the Brillouin zone (BZ) sampling, we have used the Monkhorst–Pack K -points meshes³⁴ of 0.0625 \AA^{-1} . The self-consistent convergence of the total energy was chosen to be $1.0 \times 10^{-6} \text{ eV/atom}$. For DFT calculations of the perfect and imperfect $\text{In}_x\text{Tl}_{1-x}\text{I}$ SSS the supercells, representing $3 \times 1 \times 3$ unit cells containing 72 atoms, were created. The crystal symmetry of the optimized perfect $\text{In}_x\text{Tl}_{1-x}\text{I}$ SSS at $x = 0.5$ is lower (No. 38, *Amm2*) than the space group of symmetry for InI or TII crystals (No. 63, *Cmcm*). The geometry optimization of lattice parameters and internal atomic coordinates were determined using the Broyden–Fletcher–Goldfarb–Shanno minimization technique (BFGS) with the maximum ionic Hellmann–Feynman forces within 0.02 eV/\AA , the maximum ionic displacement within $1.0 \times 10^{-3} \text{ \AA}$, and the maximum stress within 0.05 GPa . The inter- and intra-band electron transitions were calculated using the OptaDOS code.³⁵

The effective mass tensor m_{ij}^* was calculated using the Effective Mass Calculator (EMC) code³⁶ at the bands extrema using finite difference method with the step value of 0.02 (Bohr^{-1}).

RESULTS AND DISCUSSION

The crystal structure of $\text{In}_{0.5}\text{Tl}_{0.5}\text{I}$ SSS has been obtained by the replacement of two indium atoms by the thallium ones in the conventional unit cell of InI (In_4I_4). For the purpose of the proper BZ sampling of the crystals studied using the 'SeeK-path' tool³⁷ the sequence of the Cartesian axes and corresponding unit cell dimensions and atomic coordinates has been changed to satisfy the relation $a(X) < b(Y) < c(Z)$, where $a = 4.763$, $b = 4.909$, $c = 12.781$ Å.

Symmetry requirements of $\text{In}_{0.5}\text{Tl}_{0.5}\text{I}$ crystal (space group No. 38) of the unit cell content $\text{In}_2\text{Tl}_2\text{I}_4$ cause that x - and y -conventional coordinates of each atom remain constant (0.0, 0.25, 0.5 or 0.75), and only the z -coordinates of atoms may change during structure optimization together with the unit cell dimensions a , b and c . We have found, however, that the parameter of the unit cell elongation $2c/(a + b)$ of the optimized $\text{In}_2\text{Tl}_2\text{I}_4$ crystal (2.638) is close to the similar values in In_4I_4 (2.645) and Tl_4I_4 (2.638) ones.

We have also studied the imperfect $\text{In}_{0.5}\text{Tl}_{0.5}\text{I}$ SSS: with iodine vacancy (1) and with thallium interstitial atom (2). To prevent the direct interaction between neighboring iodine vacancies or thallium interstitials the supercell $3 \times 1 \times 3$ of the nominal crystal InTlI_2 with the optimized dimensions $a = 14.118$ Å, $b = 12.996$ Å, $c = 14.373$ Å (Fig. 1a) has been used for calculations. To study the interstitial structure defect in the crystal studied we have used the initial structure $\text{In}_{18}\text{Tl}_{18}\text{I}_{36}$ (supercell $3 \times 1 \times 3$), to which one thallium atom Tl_{19} has been added into the supercell center corresponding to its most probable localization (Fig. 1a).

For the cases of the primitive unit cells used (In_2I_2 , InTlI_2 , Tl_2I_2), the calculated band gap E_g of InI has been found to be indirect. In turn, the direct band gaps E_{gd} have been detected for $\text{In}_{0.5}\text{Tl}_{0.5}\text{I}$ and TlI crystals, which are not located at Γ -point of BZ (Fig. 2). For InTlI_2 the direct energy band gap E_{gd} is realized at the K -point-1/2, 1/2, 1/3 at the boundary of the first BZ, not at the Γ -point 0,0,0 (Fig. 2). The value of band gap found, $E_g = 1.31$ eV, may correspond to either direct or indirect electron transitions (Fig. 2). The inverse proportional dependence between the content index x ($\text{In}_x\text{Tl}_{1-x}\text{I}$) and the band gap E_g is observed, $E_g(x = 0) = 2.2$ eV, $E_g(x = 0.5) = 1.31$ eV, $E_g(x = 1.0) = 0.61$ eV (see Table 1), are in agreement with the previous results.¹⁶ Clear dependence between Hirshfeld charges of ions in In_2I_2 , InTlI_2 and Tl_2I_2 crystals and their band gap values is observed (Table I). In InTlI_2 SSS, the smallest interatomic distance $d_{\text{In-I}} = 3.13$ Å is smaller than the corresponding value in InI (3.22 Å), and the smallest distance $d_{\text{Tl-I}} = 3.33$ Å is larger than

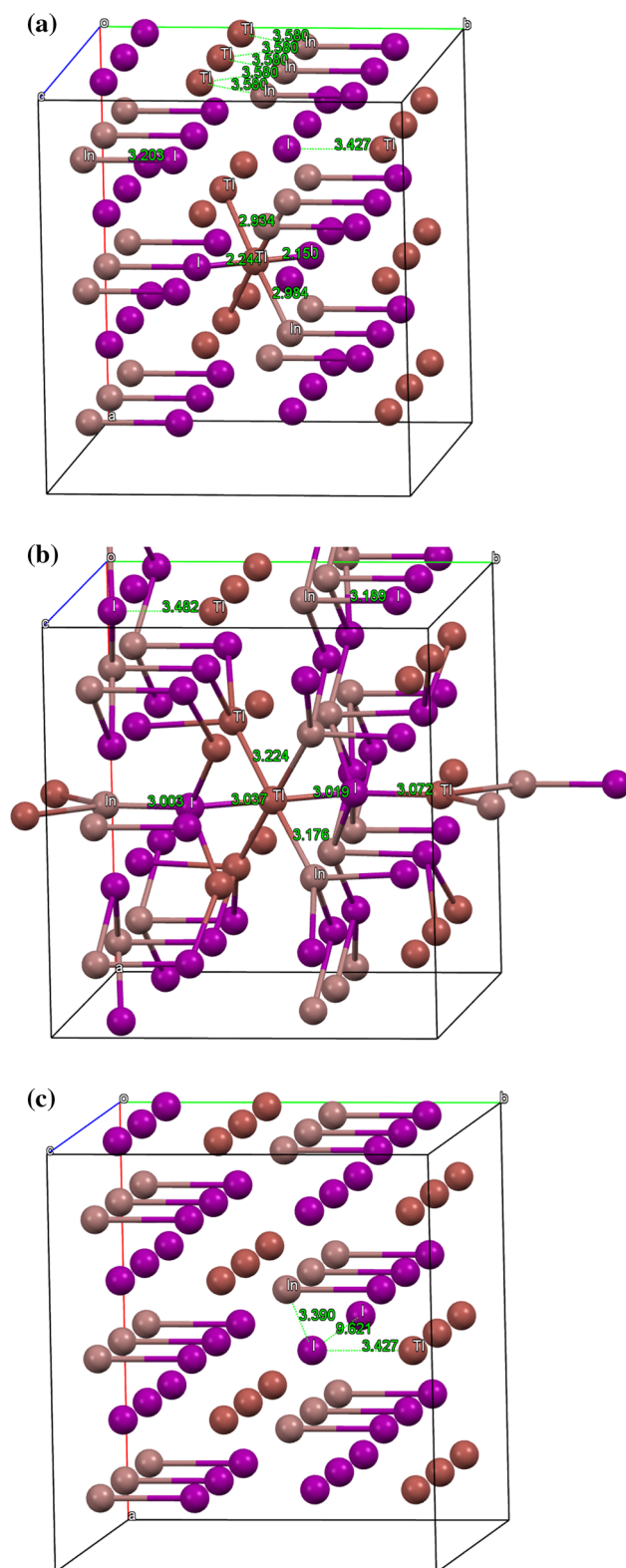


Fig. 1. Perspective views of the initially optimized structure of $\text{In}_{18}\text{Tl}_{18}\text{I}_{36}$ crystal (supercell dimensions $a = 14.118$ Å, $b = 12.996$ Å, $c = 14.373$ Å and density $\rho = 6.494$ g cm^{-3}) with additionally inserted thallium atom ($\text{In}_{18}\text{Tl}_{19}\text{I}_{36}$) before (a) and after (b) optimization and $\text{In}_{18}\text{Tl}_{18}\text{I}_{35}$ crystal with iodine vacancy (c) in the supercell $3 \times 1 \times 3$. Magnitudes of characteristic interatomic distances Tl-I , Tl-In , I-I and In-I are indicated in Angstrom units.

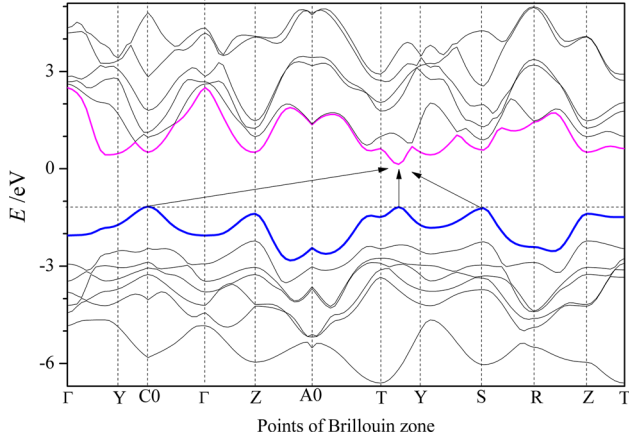


Fig. 2. Band structure of InTlI₂ SSS. Top VB and bottom CB are indicated by color lines. Probable transitions corresponding to the band gap $E_g = 1.31$ eV are shown by arrows. The K -points list used, Γ —0,0,0; Y—1/2,1/2,0; C0—0.286,0.714,0; Γ —0,0,0; Z—0,0,1/2; A0—0.286,0.286,1/2; T—1/2,1/2,1/2; Y—1/2,1/2,0; S—0,1/2,0; R—0,1/2,1/2; Z—0,0,1/2; T—1/2,1/2,1/2 corresponds to the space group of symmetry No. 38 ($Amm2$).

Table I. The Hirshfeld charges q and smallest interatomic distances d for In₂I₂, InTlI₂ and Tl₂I₂ crystals calculated at primitive unit cell

Crystal value	In ₂ I ₂	InTlI ₂	Tl ₂ I ₂
q_{In1} or q_{Tl1}/e	0.11	0.12 (In)	0.14
q_{In2} or q_{Tl2}/e	0.11	0.13 (Tl)	0.14
q_{I1}/e	-0.11	-0.13	-0.14
q_{I2}/e	-0.11	-0.12	-0.14
$d_{\text{In-I}}/\text{\AA}$	3.22	3.13	—
$d_{\text{Tl-I}}/\text{\AA}$	—	3.33	3.23
E_g/eV	0.61	1.31	2.2

the similar one in TlI (3.23 Å). This may be explained using the electronegativity values for indium (1.7), thallium (1.8) and iodine (2.5) atoms.³⁸ The larger the difference of the electronegativity values of two atoms the larger the ionicity of the corresponding chemical bond. In view of the prevailing ionic bonding in the crystals studied, one may expect the larger ion-ion interactions In-I in comparison to Tl-I, that leads to the mentioned above changes of the equilibrium interatomic distances in InTlI₂ in comparison to In₂I₂ and Tl₂I₂.

Another characteristic property of the band structure of semiconductors is the tensor of effective electron mass m_{ij}^* ,³⁹

$$(m^{*-1})_{ij} = \frac{1}{\hbar^2} \frac{\partial^2 E}{\partial K_i \partial K_j}, \quad (1)$$

which is usually presented in terms of the free electron mass m_e . Information on the effective electron mass m^* may be important because this parameter determines the dynamics of electron conductivity in material and, therefore, may be significant for the practical applications of

semiconductors. Using the EMC code,³⁶ we have found that the minimum absolute values of the components the effective mass tensor m_{ij}^* ($i, j = 1, 2, 3$) for the top VBs and bottom CBs are similar: $m_{\text{val}}^* = -0.025$ and $m_{\text{cond}}^* = 0.028$. This result forecasts the values of electron and hole conductivities in the crystals studied to be of the same order of magnitude. No clear dependences of the effective mass m^* on the content parameter x have been found for In _{x} Tl_{1- x} I. Only a weak tendency of the absolute value of effective mass decrease with increase of the content index x has been detected.

On the basis of the crystal In₁₈Tl₁₈I₃₆ described above two imperfect crystals, In₁₈Tl₁₈I₃₅, with iodine vacancy (Fig. 1c) and In₁₈Tl₁₉I₃₆ (Fig. 1a) with interstitial thallium atom have been studied.

Because of the large size of thallium atom and the interstitial character of the corresponding defect, the interatomic distances of the interstitial Tl19 atom to the surrounding iodine and indium ones are smaller (Fig. 1b) than the analogous values in the perfect crystal In₁₈Tl₁₈I₃₆ (Fig. 1a). The absolute values of Hirshfeld charges for the interstitial Tl19 ion ($q_{\text{Tl19}} = 0.02$) is seven times smaller than for the lattice site thallium ones ($q_{\text{Tl}} = 0.14$). This leads to the conclusion that the electron charge transfer between the interstitial Tl19 thallium ion and neighboring ones is much smaller than for the thallium ions of the main crystal lattice sites. Consequently, this predicts the weakening of the ionic type bonding of the interstitial Tl19 thallium atom with neighboring iodine ones, that may cause increase of the self-diffusion coefficient for thallium ions in the crystal In₁₈Tl₁₉I₃₆. The weakening of the ionic bonding of the interstitial Tl19 thallium ion with the neighboring iodine ones is also derived from the decrease of the absolute value of negative charge ($\Delta q_{\text{Tl}} = 0.01-0.02$) of the neighboring two iodine ions I25 and I33 (Fig. 1b). To obtain support of the above mentioned supposition related to the increase of the self-diffusion coefficient for thallium atom Tl19 we have performed the DFT-based molecular dynamics at the canonical NVT ensemble of the crystal In₁₈Tl₁₉I₃₆ and have found the increased mobility of Tl19 in comparison to that for the rest eighteen thallium atoms (Fig. 3).

When the supercell $3 \times 1 \times 3$ of the perfect In_{0.5}Tl_{0.5}I SSS crystal was used (Fig. 1), the direct energy band gap $E_g = 1.31$ eV has been found but to be at Γ point of BZ (Fig. 4a). This value of E_g is same as that obtained for the primitive unit cell of the crystal (Fig. 2).

Band structures of the crystals In₁₈Tl₁₈I₃₅, with iodine vacancy (Fig. 4b), and In₁₈Tl₁₉I₃₆, with thallium interstitial defect (Fig. 4c), are similar to that of the perfect one In₁₈Tl₁₈I₃₆ (Fig. 4a). One of the main differences is the larger number of energy bands in the cases of In₁₈Tl₁₈I₃₅ (Fig. 4b) and In₁₈Tl₁₉I₃₆ (Fig. 4c) comparing to In₁₈Tl₁₈I₃₆ (Fig. 4a). This feature may be caused by the energy levels

degeneracy removal due to the lower crystal symmetries of $\text{In}_{18}\text{Tl}_{18}\text{I}_{35}$ and $\text{In}_{18}\text{Tl}_{19}\text{I}_{36}$, when compared to $\text{In}_{18}\text{Tl}_{18}\text{I}_{36}$. The other main consequence of creation of the vacancy or interstitial structure defects in the $\text{In}_{18}\text{Tl}_{18}\text{I}_{36}$ crystal by changing its content to $\text{In}_{18}\text{Tl}_{18}\text{I}_{35}$ or $\text{In}_{18}\text{Tl}_{19}\text{I}_{36}$, correspondingly, is the forming of additional half-filled VBs indicated by the red lines in Fig. 4b and c. In both cases, the created half-filled VBs are located very close to the CBs in comparison to the filled valence ones. This may cause increase of the electron/hole conductivity in these imperfect crystals. In the case of the iodine vacancy defect ($\text{In}_{18}\text{Tl}_{18}\text{I}_{35}$), the energy gap between the half-filled and CBs ($\Delta E_{\text{vc}} \approx 0.2$ eV)

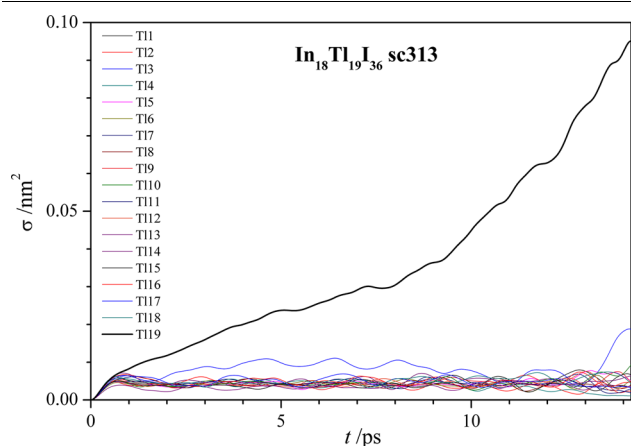


Fig. 3. Time dependence of mean square displacement $\sigma(t)$ for thallium ions in the imperfect crystal $\text{In}_{18}\text{Tl}_{19}\text{I}_{36}$ obtained at the temperature 400 K (NVT ensemble). Thick black line indicates the curve corresponding to the thallium Tl19 ion.

is larger than that, $\Delta E_{\text{vc}} \leq 0.05$ eV, in the case of the thallium interstitial defect ($\text{In}_{18}\text{Tl}_{19}\text{I}_{36}$).

One more feature of the energy band structures of the imperfect crystals studied is the smaller dispersion $E(K)$ of the top filled VB at the energy $E \approx -1.3$ eV in the crystal $\text{In}_{18}\text{Tl}_{19}\text{I}_{36}$ with thallium interstitial (Fig. 4c) in comparison to the crystal $\text{In}_{18}\text{Tl}_{18}\text{I}_{35}$ with iodine vacancy (Fig. 4b). This feature is generally in agreement with the mentioned above decrease of Hirshfeld charge of the thallium ion Tl19, which leads to the weakening of interatomic bonds in the vicinity of this ion and consequently to the increase of the corresponding electronic states localization leading in turn to the smaller dispersion $E(K)$.

Analysis of the partial density of states (PDOS) of the nominally pure $\text{In}_{18}\text{Tl}_{18}\text{I}_{36}$ and imperfect crystals $\text{In}_{18}\text{Tl}_{18}\text{I}_{35}$ and $\text{In}_{18}\text{Tl}_{19}\text{I}_{36}$ has revealed that the VB top states are created mainly (about 80%) by the electronic p -states of iodine and s -states of indium, which are hybridized strongly, the participation of thallium states are here smaller by one order of magnitude (Fig. 5). The latter is evidently caused by the smaller interatomic I-In distances in comparison to the I-Tl ones (Fig. 1). The bottom CBs of the crystals studied are created mainly (about 80%) by the strongly hybridized electronic p -states of indium and thallium, the participation of iodine states here is much smaller.

Two other main differences between PDOS observed for $\text{In}_{18}\text{Tl}_{18}\text{I}_{35}$ and $\text{In}_{18}\text{Tl}_{19}\text{I}_{36}$ clusters (Fig. 5) may be noticed. First, PDOS p -In and p -Tl in $\text{In}_{18}\text{Tl}_{19}\text{I}_{36}$ crystal at the Fermi energy are larger than the similar values in $\text{In}_{18}\text{Tl}_{18}\text{I}_{35}$ one. Second, in $\text{In}_{18}\text{Tl}_{19}\text{I}_{36}$, PDOS p -Tl is larger than p -In, when

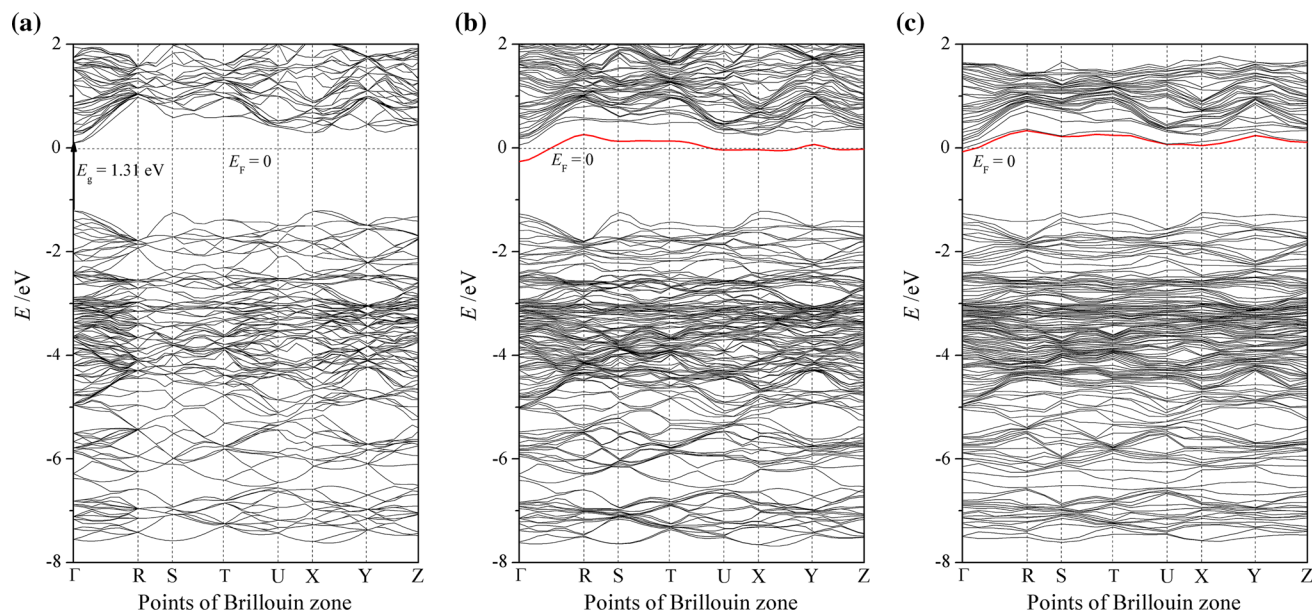


Fig. 4. Band structures of (a) $\text{In}_{18}\text{Tl}_{18}\text{I}_{36}$, (b) $\text{In}_{18}\text{Tl}_{18}\text{I}_{35}$ and (c) $\text{In}_{18}\text{Tl}_{19}\text{I}_{36}$ crystals. The Fermi level E_F is indicated by horizontal dashed lines and the top half-occupied VBs are shown by thick red lines. The set of BZ points $\Gamma-0,0,0$; $R-1/2,1/2,1/2$; $S-1/2,1/2,0$; $T-0,1/2,1/2$; $U-1/2,0,1/2$; $X-1/2,0,0$; $Y-0,1/2,0$; $Z-0,0,1/2$; corresponds to the space group of symmetry No. 25 ($Pmm2$).

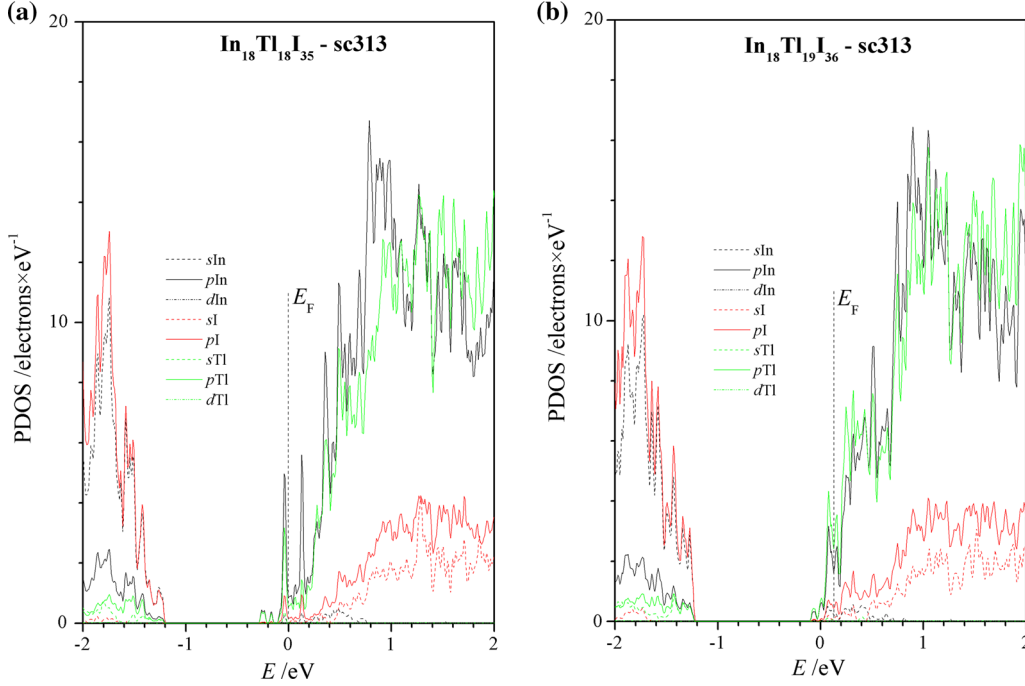


Fig. 5. Partial densities of states of $\text{In}_{18}\text{Tl}_{18}\text{I}_{35}$ with iodine vacancy (a) and $\text{In}_{18}\text{Tl}_{19}\text{I}_{36}$ with thallium interstitial (b). The Fermi energy E_F is indicated by vertical dashed lines.

in $\text{In}_{18}\text{Tl}_{18}\text{I}_{35}$, PDOS $p\text{-Tl}$ is smaller than $p\text{-In}$. These features may generally be explained by the larger number of electrons in $\text{In}_{18}\text{Tl}_{19}\text{I}_{36}$ (733) in comparison to $\text{In}_{18}\text{Tl}_{18}\text{I}_{35}$ (713).

For the imperfect crystals $\text{In}_{18}\text{Tl}_{18}\text{I}_{35}$ and $\text{In}_{18}\text{Tl}_{19}\text{I}_{36}$ the Fermi level E_F is located near the CBs bottom (Figs. 4 and 5), that means an appearance of the donor states with only one electron at the VB top. As a result, the increased electron conductivity is expected in the imperfect crystals $\text{In}_{18}\text{Tl}_{18}\text{I}_{35}$ and $\text{In}_{18}\text{Tl}_{19}\text{I}_{36}$, caused by the intra- and inter-band electron transitions. Taking into account the relation between conductivity σ and electric permittivity ε ,

$$\sigma = \sigma_1 + i\sigma_2 = -i\frac{\nu}{2}(\varepsilon_1 + i\varepsilon_2 - 1), \quad (2)$$

the spectral features of the imaginary part of dielectric function $\varepsilon_2(h\nu)$ at small photon energies are expected to be more pronounced than those for the real part of conductivity $\sigma_1(h\nu)$. In the case of the imperfect crystals $\text{In}_{16}\text{Tl}_{16}\text{I}_{31}$ and $\text{In}_{16}\text{Tl}_{17}\text{I}_{32}$, the total dielectric function $\varepsilon(h\nu)$ is a sum of two components corresponding to the inter- and intra-band electron transitions,

$$e(h\nu) = e_{\text{inter}}(h\nu) + e_{\text{intra}}(h\nu). \quad (3)$$

Here, the intra-band component $e_{\text{intra}}(h\nu)$ is usually associated with the low frequency and stationary electron conductivity, which is observed mainly in metals and heavily doped semiconductors and is

described satisfactorily by the monotonous Drude frequency dependence.⁴⁰

In view of the further discussion of the imperfect $\text{In}_{0.5}\text{Tl}_{0.5}\text{I}$ SSS we have decomposed the CASTEP-calculated dielectric function $\varepsilon(h\nu)$ of the perfect and imperfect SSS in two parts, corresponding to the inter- and intra-band electron transitions, using the OptaDOS code.²⁶ The intra-band part of dielectric function $\varepsilon_{\text{intra}}(h\nu)$ was approximated by the following relation according to the Drude model,³⁹

$$\varepsilon_{\text{intra}}(\nu) = 1 - \frac{\nu_p^2}{\nu^2 + i\gamma\nu}, \quad (4)$$

where the broadening constant $\gamma = 10^{14} \text{ s}^{-1}$ was used. The larger the plasmon frequency ν_p , the larger the imaginary part of the dielectric function $\varepsilon_{2\text{intra}}$ at the frequency $\nu = 0$, and the larger the expected direct (stationary) electron conductivity $\sigma_{1\text{intra}}(0)$.

The polarized imaginary parts of dielectric functions $\varepsilon_2(h\nu)$ for the SSS studied are shown in Fig. 6. For the inter-band electron transitions, the dielectric function $\varepsilon_2(h\nu)$ of the perfect $\text{In}_{18}\text{Tl}_{18}\text{I}_{36}$ reveals large anisotropy in the range of the band gap, $h\nu \geq E_g = 1.31 \text{ eV}$, which appears in the low-energy shift of the dependence $\varepsilon_{2z}(h\nu)$ relating $\varepsilon_{2x}(h\nu)$ and $\varepsilon_{2y}(h\nu)$ ones (Fig. 6a). The largest values of the intra- and inter-band components of $\varepsilon_{2z}(h\nu)$ at the beginning of the fundamental optical absorption, $\nu \geq 1 \text{ eV}$ (Fig. 6a), may be associated with the infinite—In—Tl—In—chains along z -axis with the smallest inter-atomic distances of 3.58 Å in the structure of the

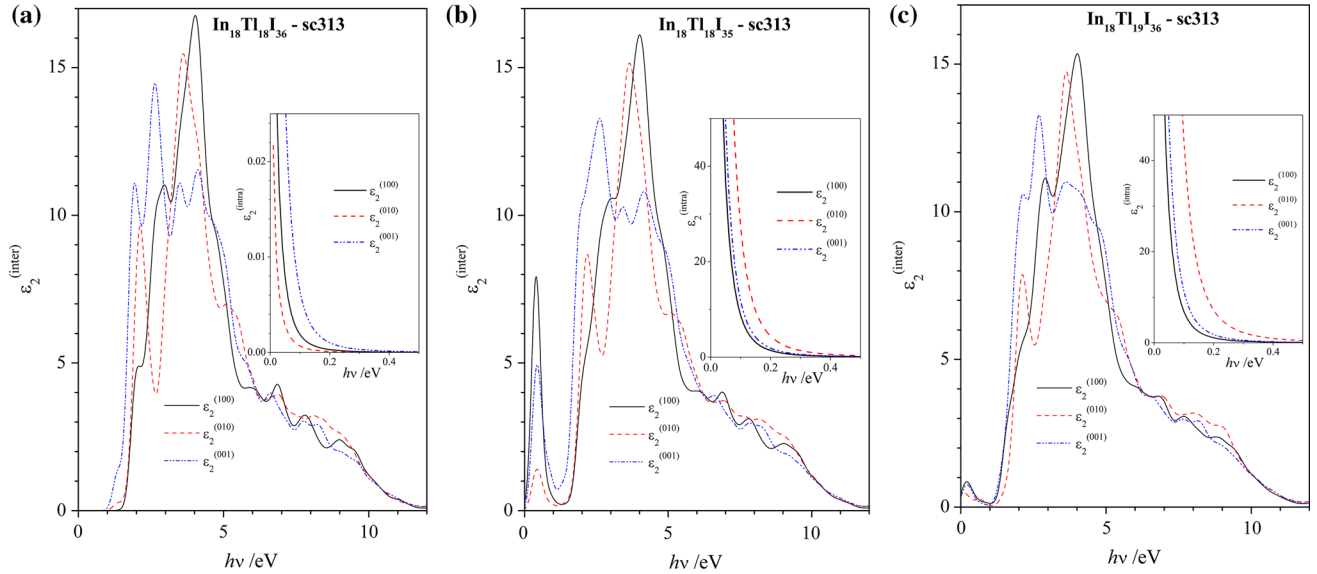


Fig. 6. Polarized imaginary parts of dielectric functions $\epsilon_2^{(\text{inter})}(h\nu)$ for the inter-band electronic transitions of $\text{In}_{18}\text{Tl}_{18}\text{I}_{36}$ (a), $\text{In}_{18}\text{Tl}_{18}\text{I}_{35}$ (b), $\text{In}_{18}\text{Tl}_{19}\text{I}_{36}$ (c) crystals. In the insets, the corresponding dependences $\epsilon_2^{(\text{intra})}(h\nu)$ for the intra-band electronic transitions in the photon energy range 0–0.5 eV.

crystals studied (Fig. 1a). This is in agreement with the site and orbital origin of PDOS for the VBs and CBs of the crystals (Fig. 5). There are no inter-band transitions in the spectral range 0–1.0 eV (Fig. 6a) and the magnitudes $\epsilon_2^{(\text{intra})}$ of the intra-band transitions in the photon energy range 0–0.5 eV are relatively small in comparison to the imperfect crystals $\text{In}_{18}\text{Tl}_{18}\text{I}_{35}$ (Fig. 6b) and $\text{In}_{18}\text{Tl}_{19}\text{I}_{36}$ (Fig. 6c).

Comparison of the dielectric functions $\epsilon_2^{(\text{inter})}(h\nu)$ of $\text{In}_{18}\text{Tl}_{18}\text{I}_{35}$ and $\text{In}_{18}\text{Tl}_{19}\text{I}_{36}$ crystals in the photon energy range 0–1.0 eV (Fig. 6b and c) with the corresponding band structures (Figs. 4b, 4c) permit claiming that the spectrum $\epsilon_2^{(\text{inter})}(h\nu)$ in this narrow range is formed by the electron transitions between the half-occupied VB top and the lowest CBs. In turn the dependences $\epsilon_2^{(\text{intra})}(h\nu)$ in the range 0–0.5 eV are formed by the intra-band electron transitions within the half-occupied top VB (see insets of Fig. 6b and c). As expected, the values of $\epsilon_2^{(\text{intra})}$ for the imperfect crystals $\text{In}_{18}\text{Tl}_{18}\text{I}_{35}$ and $\text{In}_{18}\text{Tl}_{19}\text{I}_{36}$ (Figs. 6b and c) are three orders of magnitude larger than those for the perfect one $\text{In}_{18}\text{Tl}_{18}\text{I}_{36}$ (Figure 6a).

The inverse dependences take place between the maxima of the polarized values of $\epsilon_2^{(\text{inter})}$ and $\epsilon_2^{(\text{intra})}$ in the range 0–1.0 eV (Fig. 6b and c). This looks like the sum of probabilities of the intra- and inter-band electron excitations in the range 0–1.0 eV remains constant in the imperfect crystals $\text{In}_{18}\text{Tl}_{18}\text{I}_{35}$ and $\text{In}_{18}\text{Tl}_{19}\text{I}_{36}$.

Large difference, about one order of magnitude, of the maximum the $\epsilon_2^{(\text{inter})}$ values in the range 0–1.0 eV is observed for two imperfect crystals $\text{In}_{18}\text{Tl}_{18}\text{I}_{35}$ and $\text{In}_{18}\text{Tl}_{19}\text{I}_{36}$ (Fig. 6b, c). The possible explanation of the much smaller $\epsilon_2^{(\text{inter})}$ magnitudes in $\text{In}_{18}\text{Tl}_{19}\text{I}_{36}$ at the range 0–1.0 eV may be that the

probabilities of the interband and intraband excitations are close one to another due to the close vicinity of the band energies of the half-filled VBs and non-filled CBs (see Fig. 4c). The proposed model of dividing the absorbed photon energy into two paths, corresponding to the inter- and intra-band transitions, is found to be valid for every polarized component of the electric permittivities $\epsilon_{2i}^{(\text{inter})}$ and $\epsilon_{2i}^{(\text{intra})}$ ($i = x, y, z$) (Fig. 6b and c).

CONCLUSIONS

The DFT-based calculations of the band electronic structure and dielectric function have been performed for both the perfect and imperfect (with iodine anion vacancy and thallium cation interstitial) of $\text{In}_{0.5}\text{Tl}_{0.5}\text{I}$ SSS. On the basis of the band structures obtained, the tensors of effective electron mass have been calculated for the perfect InI, $\text{In}_{0.5}\text{Tl}_{0.5}\text{I}$ and TII crystals. Absolute values of the effective electron masses for the perfect crystals studied have been found to be of the same order of magnitude. Minor decrease of the averaged effective electron masses takes place in the direction $\text{TII} \rightarrow \text{In}_{0.5}\text{Tl}_{0.5}\text{I} \rightarrow \text{InI}$.

Insertion of the iodine vacancy or thallium interstitial into the nominal $\text{In}_{0.5}\text{Tl}_{0.5}\text{I}$ SSS, taken in the form of the $3 \times 1 \times 3$ supercell, leads to the appearance of the half-filled energy band located in the energy range of the band gap $E_g = 1.31$ eV of the perfect crystal closer to the corresponding CBs.

Imaginary parts of the dielectric functions calculated for the imperfect $\text{In}_{0.5}\text{Tl}_{0.5}\text{I}$ SSS with the iodine vacancy or thallium interstitial possess the considerable, in comparison to the corresponding perfect crystal, low-frequency inter-band and intra-band components in the photon energy range $h\nu <$

1.0 eV. This indicates a presence of the low-frequency and stationary electron conductivity in the imperfect $\text{In}_{0.5}\text{Tl}_{0.5}\text{I}$ crystals.

The present results of the DFT-based calculations of InI-TII SSS physical properties may serve as the basis for the future similar studies of these materials and improvements of the investigational methods by studying the influence on the materials structural and optical parameters of the electric,⁴¹ magnetic²⁹ fields and nanoparticles.¹ The obtained results of the bulk properties of the titled crystals can be used in further studies of surface phenomena⁴² in the corresponding thin film structures.

ACKNOWLEDGMENTS

Computer calculations have been performed using the Academic release of the CASTEP code (ver. 18.1) at WCSS of Wrocław University of Technology, Poland (project No. 053). The work was supported by the Project of Young Scientists (Co-66Hp) of Ukraine.

OPEN ACCESS

This article is distributed under the terms of the Creative Commons Attribution 4.0 International License (<http://creativecommons.org/licenses/by/4.0/>), which permits unrestricted use, distribution, and reproduction in any medium, provided you give appropriate credit to the original author(s) and the source, provide a link to the Creative Commons license, and indicate if changes were made.

REFERENCES

- R. Iovine, L. La Spada, and L. Vegni, *Adv. Nanoparticles* 2, 21 (2013).
- I. Liberal and N. Engheta, *Nat. Photon.* 11, 149 (2017).
- L. La Spada, *Sensors* 19, 355 (2019).
- A. Vakil, *Science* 332, 1291 (2011).
- R. Iovine, L. La Spada, R. Tarparelli, and L. Vegni, *Mater. Sci. Forum* 792, 110 (2014).
- M.G. Kanatzidis, *Inorg. Chem.* 56, 3158 (2017).
- I. Chung, G. Mercouri, and M.G. Kanatzidis, *Chem. Mater.* 26, 849 (2014).
- M. Piasecki, M.G. Brik, I.E. Barchiy, K. Ozga, I.V. Kityk, A.M. Al-Naggar, A.A. Albassam, T.A. Malakhovskaya, and G. Lakshminarayana, *J. Alloys Compd.* 710, 600 (2017).
- M. Piasecki, G.L. Myronchuk, O.V. Zamurueva, O.Y. Khyzhun, O.V. Parasyuk, A.O. Fedorchuk, A. Albassam, A.M. El-Naggar, and I.V. Kityk, *Mater. Res. Express* 3, 025902 (2016).
- M.G. Brik, M. Piasecki, and I.V. Kityk, *Inorg. Chem.* 53, 2645 (2014).
- V.V. Atuchin, Yu.M. Andreev, S.A. Bereznaya, T.A. Gavrilova, G.V. Lanskiy, T.D. Malinovskaya, A.N. Morozov, Z.V. Korotchenko, L.D. Pokrovsky, S.Yu. Sarkisov, in *Siberian Conference on Control and Communications* (2007), pp. 179-184.
- Q. Guo, A. Assoud, and H. Kleinke, *Materials Aspect of Thermoelectricity*, ed. C. Uher (Boca Raton: CRC Press, 2016).
- I.V. Blonsky, M.I. Kolinko, YuO Lun, and A.V. Franiv, *Proc. SPIE* 2647, 452 (1995).
- A. Franiv, R. Peleshchynshyn, and Y. Kolosivski, *Ukr. J. Phys. Opt.* 1, 24 (2000).
- Y.O. Dovhyi, A.V. Franiv, and S.V. Ternavska, *Ukr. J. Phys. Opt.* 2, 141 (2001).
- A.I. Kashuba, M. Piasecki, O.V. Bovgyra, V.Y. Stadnyk, P. Demchenko, A. Fedorchuk, A.V. Franiv, and B. Andriyevsky, *Acta Phys. Pol., A* 133, 68 (2018).
- M.S. Brodin, I.V. Blonskii, B.M. Nitsovich, A.S. Krochuk, and A.V. Franiv, *Phys. Status Solidi B* 111, 625 (1982).
- R. Zallen and M.L. Slade, *Solid State Commun.* 17, 1561 (1975).
- A.V. Franiv, A.I. Kashuba, and O.V. Bovgyra, Patent of Ukraine, Bulletin No. 16, published on 2017-08-28 (<http://base.uipv.org/searchINV/>), application number u201702658).
- L. Helmholz and Z. Kristallogr, *Krist.* 95, 129 (1936).
- R.E. Jones and D.H. Templeton, *Acta Crystallogr.* 8, 847 (1955).
- G. Meyer, T. Staffel, and Z. Anorg, *Allg. Chem.* 574, 114 (1989).
- R.P. Lowndes and C.H. Perry, *J. Chem. Phys.* 58, 271 (1973).
- A.V. Franiv, V.Y. Stadnyk, A.I. Kashuba, R.S. Brezvin, O.V. Bovgyra, and A.V. Futei, *Opt. Spectrosc.* 123, 177 (2017).
- A.V. Franiv, A.I. Kashuba, O.V. Bovgyra, and O.V. Futei, *Ukr. Fiz. Zh.* 62, 679 (2017).
- A.I. Kashuba, A.V. Franiv, R.S. Brezvin, and O.V. Bovgyra, *Funct. Mater.* 23, 26 (2017).
- A.I. Kashuba, Ya.A. Zhydachevskyy, I.V. Semkiv, A.V. Franiv, and O.S. Kushnir, *Ukr. J. Phys. Opt.* 19, 1 (2018).
- L. La Spada, R. Iovine, and L. Vegni, *J. Res. Updates Polym. Sci.* 2, 194 (2013).
- Y.R. Padooru, A.B. Yakovlev, C.S.R. Kaipa, G.W. Hanson, F. Medina, F. Mesa, and A.W. Glisson, *IEEE Trans. Antennas Propag.* 60, 5727 (2012).
- R. Iovine, L. La Spada, R. Tarparelli, L. Vegni, SPIE, (2013) <https://doi.org/10.1117/12.2020522>.
- P. Hohenberg, W. Kohn, *Phys. Rev.* (1964) <https://doi.org/10.1103/physrev.136.b864>.
- S.J. Clark, M.D. Segall, C.J. Pickard, P.J. Hasnip, M.J. Probert, K. Refson, and M.C. Payne, *Z. Kristallogr.* 220, 567 (2005).
- J.P. Perdew, A. Ruzsinszky, G.I. Csonka, O.A. Vydrov, G.E. Scuseria, L.A. Constantin, X. Zhou, and K. Burke, *Phys. Rev. Lett.* 100, 136406 (2008).
- H.J. Monkhorst and J.D. Pack, *Phys. Rev. B* 13, 5188 (1976).
- A.J. Morris, R. Nicholls, C.J. Pickard, and J. Yates, *Comput. Phys. Commun.* 185, 1477 (2014).
- A. Fonari, C. Sutton, Effective mass calculator (2012).
- Y. Hinuma, G. Pizzi, Y. Kumagai, F. Oba, and I. Tanaka, *Comp. Mater. Sci.* 128, 140 (2017).
- L. Pauling, *The Nature of the Chemical Bond*, 3rd edn. (Cornell University, 1960).
- M. Grundmann, *The Physics of Semiconductors* (Berlin: Springer, 2006).
- H. Fujiwara, *Spectroscopic Ellipsometry: Principles and Applications* (Chichester: Wiley, The Atrium, Southern Gate, 2007).
- F. Qin, L. Ding, L. Zhang, F. Monticone, C.C. Chum, J. Deng, S. Mei, Y. Li, J. Teng, M. Hong, S. Zhang, A. Alù, and C.-W. Qiu, *Sci. Adv.* (2016). <https://doi.org/10.1126/sciadv.1501168>.
- L. La Spada, A.-M. Vegni, Latin America Optics and Photonics Conference, Th3C. 2, (2018), <https://doi.org/10.1364/laop.2018.th3c.2>.

Publisher's Note Springer Nature remains neutral with regard to jurisdictional claims in published maps and institutional affiliations.